Solar Energy Materials & Solar Cells 107 (2012) 37–45

Contents lists available at SciVerse ScienceDirect

Solar Energy Materials & Solar Cells

journal homepage: www.elsevier.com/locate/solmat

Modelling of optical durability of enhanced aluminum solar reflectors

Florian Sutter [a,*], Stefan Ziegler [b], Martin Schmücker [c], Peter Heller [a], Robert Pitz-Paal [a]

[a] DLR German Aerospace Center, Institute of Solar Research, Plataforma Solar de Almeria, Ctra. Senés Km. 5, P.O. Box 44, 04200 Tabernas, Almería, Spain
[b] Alanod Aluminium-Veredlung GmbH, Egerstraße 12, D-58256 Ennepetal, Germany
[c] DLR German Aerospace Center, Institute of Materials Research, Linder Höhe, D-51147 Cologne, Germany

ARTICLE INFO

Article history:
Received 27 March 2012
Received in revised form
20 July 2012
Accepted 25 July 2012

Keywords:
Aluminum solar reflector
Outdoor weathering
Specular reflectance
Scattering
Localized corrosion of aluminum
Avrami equation

ABSTRACT

In order to reduce electricity generation costs of concentrating solar power (CSP) technologies, new low-cost reflector materials are being developed. These materials need to withstand harsh outdoor conditions without a significant loss in specular reflectance. In this work, samples of enhanced anodized aluminum reflectors protected by a sol–gel coating that have been exposed at different weathering sites were analyzed with an innovative specular reflectometer in order to monitor corrosion and scattering caused by surface roughness. A model to estimate the specular reflectance as a function of exposure conditions at different weathering sites has been developed.

1. Introduction

Aluminum reflectors are increasingly being used in concentrated solar power applications because of their high formability and lightweight properties. They offer flexibility in the design, construction and assembly of new collectors. Because of their high ductility, aluminum mirrors will not break even at high wind loads. The manufacturing process is well suited for mass production because of the coil coating process. Consequently, aluminum reflectors offer a significant cost reduction potential compared to glass mirrors.

Enhanced first-surface aluminum mirrors are produced by anodizing a 0.5 mm-thick polished aluminum substrate. The thickness of the anodized layer is about 3 μm. Afterwards a 65 nm-thick pure aluminum layer is deposited by physical vapor deposition (PVD). The reflectance of the aluminum is enhanced by 1/4wavelength (λ) thick low-index (95 nm SiO_2) and high-index (60 nm TiO_2) refractive oxide coatings. The structure of the SiO_2 and TiO_2 films is known to be columnar and porous [1]. The coating stack is then protected with a (3 μm SiO_2) sol–gel nanocomposite oxide layer (see Figs. 1 and 2).

2. Material and methods

Enhanced aluminum reflector samples have been exposed in Almería and Tabernas (Spain), and in Florida, Golden and Arizona (USA). The degradation mechanism of the outdoor exposed samples has been analyzed with microscopy and with optical measurement devices. Scanning transmission electron microscopy (STEM) has been performed at the National Renewable Energy Laboratory (NREL) with a FEI Tecnai F20 UT in the Z-contrast mode (the intensity is proportional to the atomic number Z) with a high-angle annular dark field (HAADF) detector. Scanning electron microscopy (SEM) has been performed at the materials laboratory of DLR in Cologne with a Carl Zeiss Micro Imaging Ultra 55 FEG. The 2-D light microscope images were made with a Carl Zeiss Axio CSM 700.

The influence of the detected degradation mechanisms on the specular reflectance of the mirror was examined using a prototype of an innovative specular reflectometer. The device enables the measurement of the specular reflectance ρ at different acceptance half-angles φ. The system is based on a photographic method that allows the reflectance characteristics of flat mirrors to be evaluated at any point on its surface. It has a spatial resolution of 37 pixel/mm and a precision of $\pm 0.6\%$ at $\varphi = 12.5$ mrad acceptance half-angle [2]. Herein we denote specular reflectance as ρ ($\lambda = 656$ nm; $\theta = 15^\circ$; $\varphi = 12.5$ mrad) where λ is the wavelength and θ is the angle of incidence.

2.1. Localized corrosion of the aluminum layer

All exposed samples showed localized corrosion spots. The effect was more pronounced at the coastal sites of Almería and Florida but localized corrosion has also been detected at samples exposed in dry desert conditions. Fig. 3 shows a light microscope image of a typical corrosion spot that appeared after 64 months of outdoor exposure in Tabernas.

* Corresponding author. Tel.: +34 950 277 684; fax: +34 950 260 315.
E-mail addresses: Florian.Sutter@dlr.de (F. Sutter), Ziegler@alanod.de (S. Ziegler), Martin.Schmuecker@dlr.de (M. Schmücker), Peter.Heller@dlr.de (P. Heller), Robert.Pitz-Paal@dlr.de (R. Pitz-Paal).

0927-0248/$ - see front matter © 2012 Elsevier B.V. All rights reserved.
http://dx.doi.org/10.1016/j.solmat.2012.07.027

Nomenclature

A_C	area of a single corrosion spot (m^2)
A_{ext}	extended area of all corrosion spots (m^2)
A_{total}	total mirror surface [m^2]
c_J	nucleation rate constant [$s^{-0.5}/mm^2$]
f_C	corroded area fraction (dimensionless)
$f_{C,cont.}$	corroded area fraction for the case of continuous nucleation [dimensionless]
$f_{C,sim.}$	corroded area fraction for the case of simultaneous nucleation (dimensionless)
$f_{ext,cont.}$	extended area fraction for the case of continuous nucleation (dimensionless)
$f_{ext,sim.}$	extended area fraction for the case of simultaneous nucleation (dimensionless)
J	nucleation rate ($s^{-1}\,m^{-2}$)
k	Avrami constant (k is expressed in ($months^{-0.5}$) for an Avrami exponent of $\eta=0.5$) ($s^{-\eta}$)
m	number of dimensions (dimensionless)
m_C	constant (%/months)
m_S	constant (%/months)
N	density of nuclei ($1/m^{-2}$)
n	number of nuclei (dimensionless)
n_{ext}	number of nuclei of extended area (dimensionless)
r	radius of the corrosion spot (m)
r_{eq}	equivalent radius of the corrosion spot (m)
t	time (s)
v_C	growth velocity of a corrosion spot (m/s)
Δt	time interval between the formation of new corrosion spots (s)
$\Delta\rho_C$	specular reflectance loss caused by corrosion ($\lambda=665$ nm; $\theta=15^\circ$; $\varphi=12.5$ mrad) (%)
$\Delta\rho_S$	specular reflectance loss caused by scattering ($\lambda=665$ nm; $\theta=15^\circ$; $\varphi=12.5$ mrad) (%)
η	Avrami exponent (dimensionless)
θ	incidence angle (deg.)
λ	wavelength (nm)
ρ	specular reflectance at wavelength $\lambda=656$ nm, incidence angle $\theta=15^\circ$ and acceptance angle $\varphi=12.5$ mrad (%)
ρ_0	initial specular reflectance before outdoor weathering ($\lambda=665$ nm; $\theta=15^\circ$; $\varphi=12.5$ mrad) (%)
$\rho_{0,fC}$	constant (%)
ρ_{fC}	average specular reflectance of corroded area fraction ($\lambda=665$ nm; $\theta=15^\circ$; $\varphi=12.5$ mrad) (%)
ρ_{fS}	average specular reflectance of non-corroded area fraction ($\lambda=665$ nm; $\theta=15^\circ$; $\varphi=12.5$ mrad) (%)
φ	acceptance angle (mrad)

A STEM cross section image reveals that the degradation occurs at the pure 65 nm-thick aluminum layer (Fig. 4). STEM analysis requires very thin samples that are almost transparent for electrons. Preparation of the 100 Å thick cross section sample was performed by focused ion beam (FIB) to avoid the introduction of defects. Other attempts to prepare the sample (like polishing or grinding) were not successful because the mechanical treatment caused delamination of the sample's coating.

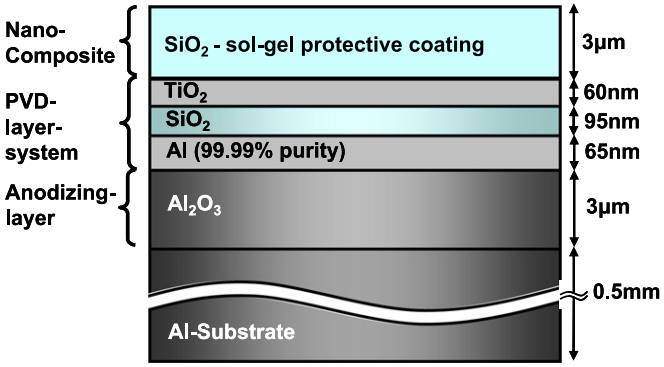

Fig. 1. Schematic composition of enhanced aluminum reflectors.

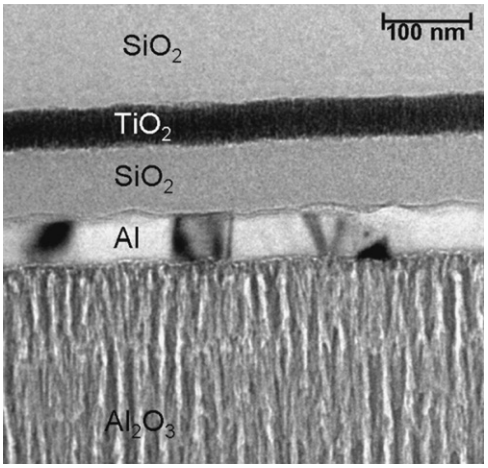

Fig. 2. Cross section viewed in a transmission electron microscope (TEM) .

A vertical energy-dispersive X-ray spectroscopy (EDX) line scan with high spatial resolution detected a loss of the aluminum in the degraded areas (as indicated by the dotted line scan in Fig.4). The left side of the STEM-image shows an unharmed region with an intact pure aluminum layer. This region is probably an "island" (compare Fig. 3).

Further microscopic analysis has shown that the corrosion starts at defects in the 3 µm-thick nanocomposite layer. Fig. 5 shows the corrosion initiation at a coating defect deliberately inserted with a scratching tool as the sample is brought in contact with a sodium chloride solution (50 g/l NaCl in demineralized water).

While the pure aluminum layer corrodes, the SiO_2 and TiO_2 enhancing layers remain almost unharmed. During the corrosion hydrogen bubbles are formed which tend to introduce microcracks or coating break outs in the overlying coatings (see Figs. 3and 5c). The observed corrosion mechanism has similarities with filiform

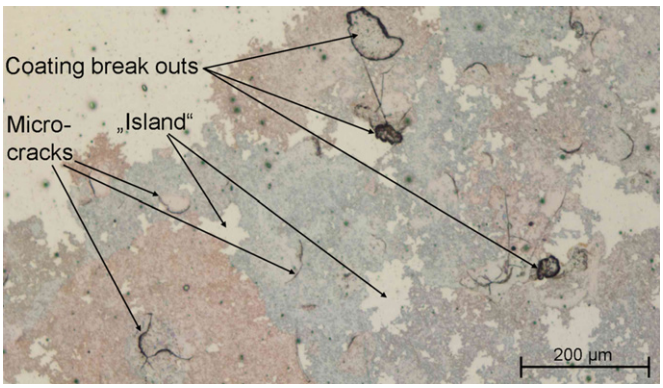

Fig. 3. Typical corrosion of outdoor exposed aluminum reflector samples.

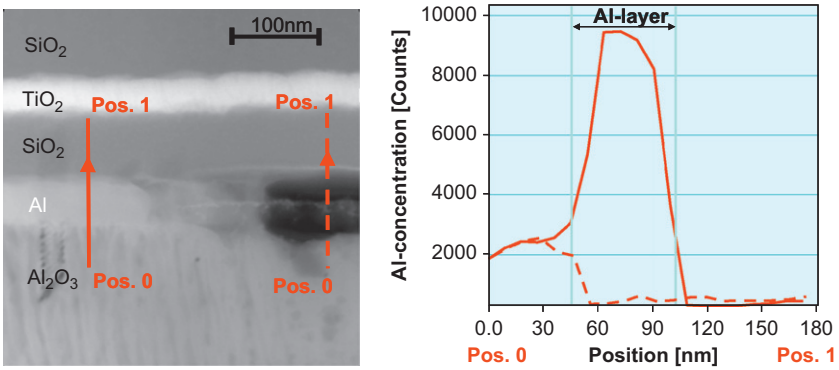

Fig. 4. Cross section image of a corrosion spot viewed in STEM (left). The EDX line scans (right) show severe aluminum loss in the affected region by corrosion (dotted line). The area not affected by corrosion shows high aluminum content (solid line).

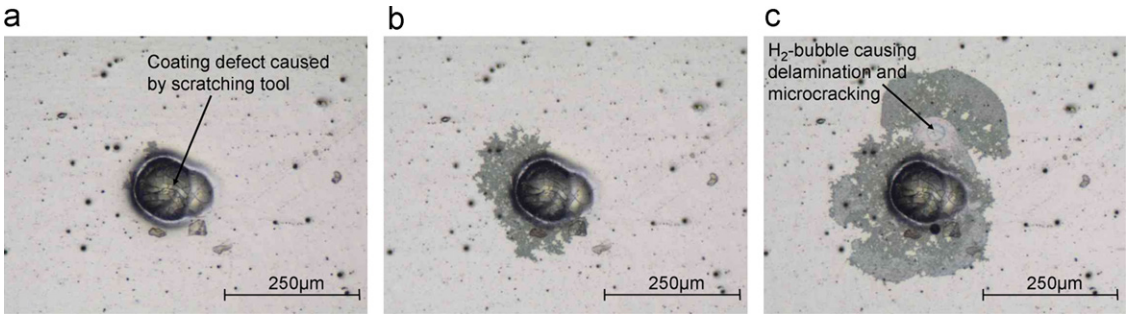

Fig. 5. Corrosion propagation when a sample is brought in contact with sodium chloride solution (50 g/l NaCl) (a) after 30 s, (b) after 12 min, and (c) after 50 min.

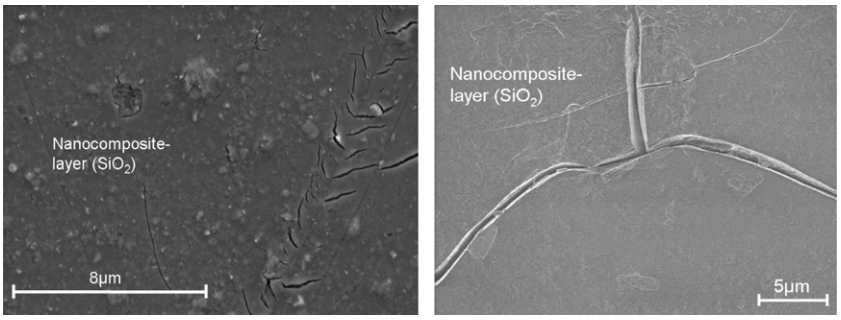

Fig. 6. Surface roughness introduced during outdoor weathering.

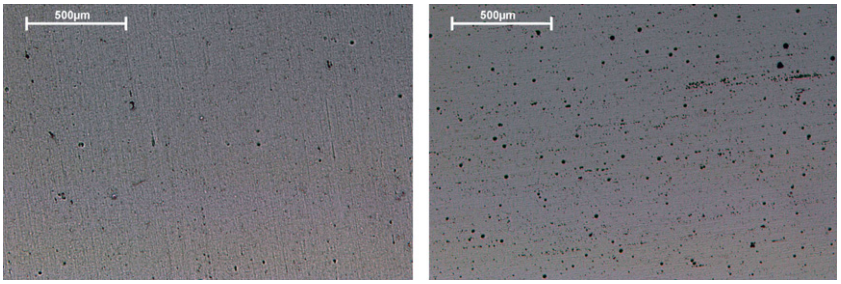

Fig. 7. (a): new, non-aged material, $\rho=85.2\%$ and (b) after 64 months of outdoor exposure in Tabernas, $\rho=81.5\%$.

corrosion, although the characteristic thread-like filaments are not observed.

2.2. Scattering

A microscopic inspection of the non-corroded surface of the exposed samples revealed that in the course of the outdoor weathering additional roughness is being introduced to the top nanocomposite coating. Smaller cracks or coating defects may not be deep enough to initiate corrosion but they will introduce scattering and lower the specular reflectance of the mirror. Fig. 6 shows scanning electron microscope (SEM) images of such defects.

Fig. 7 shows light microscope images of a new sample, compared to a sample exposed for more than 5 years outdoors in the Tabernas Desert in Spain. A high increase of the coating defect density can be observed which results in a specular

reflectance loss of about $\Delta\rho_S=3.7\%$ caused by scattering ($\lambda=656$ nm; $\theta=15^\circ$; $\varphi=12.5$ mrad).

3. Modelling specular reflectance losses

The specular reflectance over time $\rho(t)$ decreases due to the influence of different degradation mechanisms that induce a certain reflectance loss:

$$\rho(t)=\rho_0-\sum_i \Delta\rho_i(t) \tag{1}$$

where ρ_0 describes the initial specular reflectance of the mirror and $\Delta\rho_i$ describes the reflectance losses caused by various relevant degradation mechanisms. Through the microscopic analysis described before, localized corrosion and scattering caused by surface roughness have been detected as major degradation mechanisms for the enhanced aluminum reflector. Thus, Eq. (1) yields

$$\rho(t)=\rho_0-\Delta\rho_C(t)-\Delta\rho_S(t) \tag{2}$$

where $\Delta\rho_C$ describes the specular reflectance losses caused by corrosion and $\Delta\rho_S$ describes the specular reflectance losses caused by scattering.

3.1. Modelling of specular reflectance losses caused by corrosion $\Delta\rho_C$

In order to model the corroded area fraction f_c of the mirror surface the Avrami theory is used [3]. The theory is specifically modified to model the growth of localized corrosion of aluminum reflectors during outdoor weathering.

In the classical theory, Avrami distinguishes between two types of heterogeneous nucleation, depending upon whether the growth is simultaneous or continuous (see Fig. 8):

- For simultaneous nucleation all nuclei are present at the beginning of the exposure at $t=0$. The density of nuclei N results from the number of nuclei n per area unit.
- For continuous nucleation, a new nucleus is added after each delay time interval Δt. In the Avrami theory the nucleation rate J is assumed to be constant.

In order to describe those two ideal cases the following assumptions are made:

- Nuclei appear randomly over the whole reflector surface
- The processes are regarded as two-dimensional (the aluminum layer is much thinner than the extension of the corrosion spots).
- The nuclei have a constant growth velocity v_C.

The time dependent area of a single corrosion spot formed at time $t=i\Delta t$ with radius r is calculated by:

$$A_C(t)=\pi r^2(t)=\pi(v_C(t-i\Delta t))^2 \tag{3}$$

where v_C denotes the constant growth velocity of the corrosion spot. In the case of simultaneous nucleation Δt is zero.

An extended area A_{ext} is calculated (see Fig. 9), for which the corrosion would take place if

- there was no limitation of growth of the corrosion spots due to boundaries or overlapping with other spots
- there was no limitation of nucleation in an already corroded area

In the case of simultaneous nucleation the corroded extended area fraction f_{ext} is calculated by multiplying the area of single corrosion spots with the density of nuclei N:

$$f_{ext,sim.}=\frac{A_{ext}}{A_{total}}=\frac{\Sigma A_i}{A_{total}}=\frac{\pi(v_C t)^2 n}{A_{total}}=\pi(v_C t)^2 N \tag{4}$$

In the case of continuous nucleation,

$$f_{ext,cont.}=\frac{A_{ext}}{A_{total}}=\frac{1}{A_{total}}\sum_{i=0}^{n_{ext}}\pi v_C^2(t-i\Delta t)^2 \tag{5}$$

where n_{ext} denotes the number of nuclei of the extended area. In Fig. 9 for example n_{ext} would have the value of three even though only $n=2$ nuclei could be detected.

When $n_{\mathrm{ext}}=t/\Delta t$ the nucleation rate J can be expressed as:

$$J=\frac{dN_{ext}}{dt}=\frac{d(n_{ext}/A_{total})}{dt}=\frac{1}{A_{total}}\frac{dn_{ext}}{dt}=\frac{1}{A_{total}}\frac{d}{dt}\left(\frac{t}{\Delta t}\right)=\frac{1}{A_{total}\Delta t} \tag{6}$$

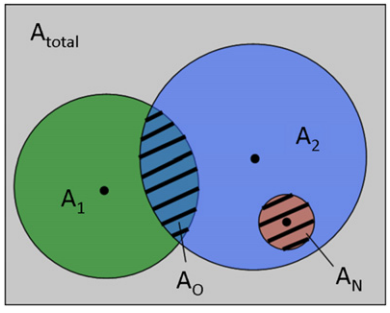

Fig. 9. Visualization of the extended area $A_{ext}=A1+A2+A_N$ which may contain overlapped surface fractions (AO) and nuclei within already corroded area (AN). The actual corroded area is $A=A1+A2-AO$.

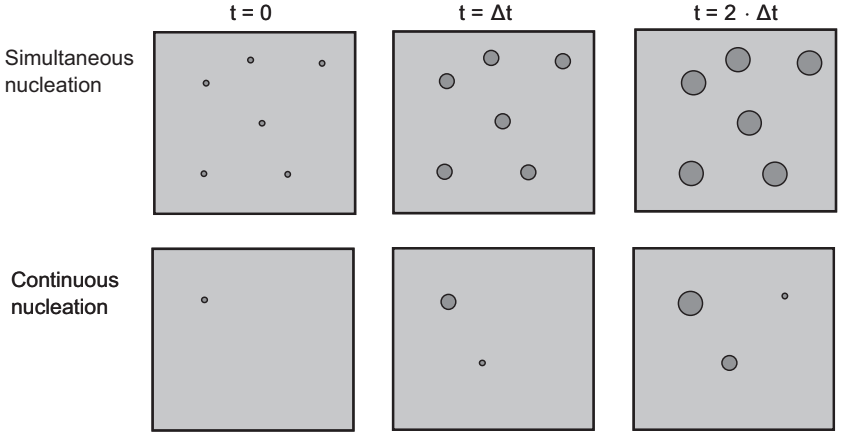

Fig. 8. Types of nucleation.

In the limiting case of $\Delta t \to 0$ the sum in Eq. (5) can be replaced by a Riemann integral:

$$f_{ext,cont.} = \lim_{\Delta t \to 0} \sum_{i=0}^{n_{ext}} \pi v_C^2 (t - i\Delta t)^2 \frac{1}{A_{total}\Delta t} \Delta t = \int_0^t \pi v_C^2 (t-t')^2 J \, dt' \quad (7)$$

Solving the integral in (7) yields

$$f_{ext,cont.} = \int_0^t \pi v_C^2 (t-t')^2 J \, dt' = -\frac{\pi v_C^2 J}{3} \left[(t-t')^3 \right]_{t'=0}^{t'=t} = \frac{\pi v_C^2 J t^3}{3} \quad (8)$$

To calculate the actual corroded area fraction f_C consider the following: at time t the corroded area fraction is denoted by f_C, therefore the non-corroded area fraction is $(1-f_C)$. In the time interval dt, f_{ext} will grow by df_{ext}. But only the non-corroded area fraction contributes to the growth of f_C. The extended area fraction f_{ext} is correlated to the actual corroded area fraction f_C by the following equation [3]:

$$df_C = (1-f_C) df_{\text{ext}} \quad (9)$$

At the beginning of outdoor exposure the corrosion grows with df_{ext} because $f_C = 0$. But with an increasing number of corrosion spots there will be less surface where new nuclei can form. This is why the corrosion per time interval dt is increasingly inhibited. Solving the differential Eq. (9) results in

$$\frac{df_C}{(1-f_C)} = df_{\text{ext}} \quad (10)$$

$$-\ln(1-f_C) = f_{\text{ext}} \quad (11)$$

The integration constant is zero because at $t=0$, f_C and f_{ext} are both zero. Solving (11) yields the two-dimensional Johnson–Mehl–Avrami–Kolmogorow (JMAK) equation [4]:

$$f_C = 1 - e^{-f_{ext}} \quad (12)$$

$$\text{For continuous nucleation}: \; f_{C,cont.} = 1 - \exp\left(-\frac{\pi v_C^2 J t^3}{3} \right) \quad (13)$$

$$\text{For simultaneous nucleation}: \; f_{C,sim.} = 1 - \exp(-\pi v_C^2 N t^2) \quad (14)$$

The general JMAK-equation is

$$f_C = 1 - e^{-kt^{\eta}} \quad (15)$$

where k denotes the Avrami constant and η the Avrami exponent. The Avrami exponent depends on the type of nucleation and the dimensions of the process (see Table 1). Fig. 10 shows the corroded area fraction f_C for different Avrami exponents.

To determine the type of growth of localized corrosion spots of enhanced aluminum reflectors several samples exposed outdoors have been analyzed periodically with the space resolved reflectometer from [2]. In addition to the reflector shown in Fig.1, some samples without the 3 µm-thick nanocomposite layer were exposed outdoors. The rest of the layer system was identical to the one shown in Fig. 1. Those samples experienced identical localized corrosion. However, the nucleation rate was much faster because of the missing protective coating. Fig. 11 shows the appearance of localized corrosion spots of an enhanced aluminum reflector sample without a nanocomposite protective top layer after 1 and 2 weeks of outdoor exposure in Almería, Spain.

Table 1
Avrami exponent η for different types of growth for constant corrosion growth velocities v_C=const. For $v_C=0$, the Avrami exponent η' results in $\eta' = \eta - m$.

Type of growth	η
Continuous nucleation	
One-dimensional ($m=1$)	2
Two-dimensional ($m=2$)	3
Tree-dimensional ($m=3$)	4
Simultaneous nucleation	
One-dimensional ($m=1$)	1
Two-dimensional ($m=2$)	2
Three-dimensional ($m=3$)	3

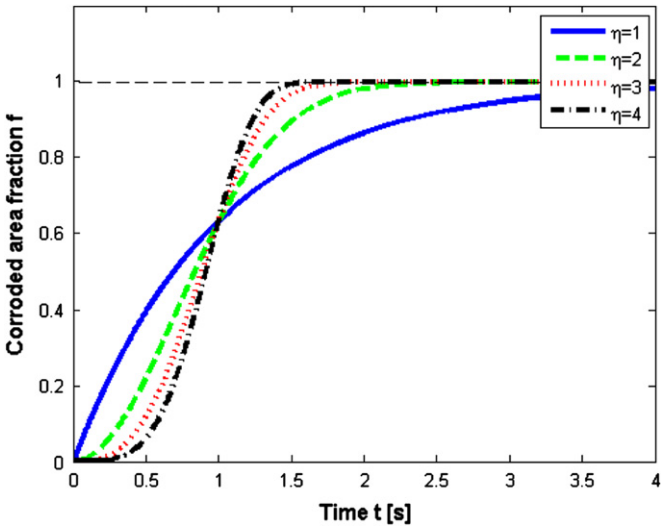

Fig. 10. Corroded area fraction for different Avrami exponents according to the JMAK-Eq. (15). The Avrami constant is $k = 1\ s^{-\eta}$.

The results show that in contrast to the cases of simultaneous and continuous nucleation described by the Avrami-theory, the growth velocity v_C of the corrosion spots is not constant. They form quickly at the beginning of exposure but after a certain time the growth stagnates and the area of the corrosion spot remains constant ($v_C=0$). In order to model this process the following simplifying assumptions were made:

- As the corrosion spots are not round they are replaced by circles of an equivalent area. The radius of the circles is denoted as r_{eq}.
- The time for a corrosion spot to grow is neglected ($v_C=0$).
- Single spots do not change in shape once they appear (r_{eq}=constant).

The area of a corrosion spot can then be calculated as

$$A_C = \pi r_{eq}^2 = \text{const.} \quad (16)$$

The extended corroded area fraction for localized corrosion of the aluminum reflector is f_{ext}:

$$f_{ext} = \frac{\Sigma_i A_{C,i}}{A_{total}} = \frac{\Sigma_{i=0}^{n_{ext}} \pi r_{eq}^2}{A_{total}} = \frac{\pi r_{eq}^2 n_{ext}}{A_{total}} = \pi r_{eq}^2 N_{ext} = \pi r_{eq}^2 J t \quad (17)$$

From (12) the corroded area fraction can be calculated as:

$$f_C = 1 - \exp(-\pi r_{eq}^2 J t) \quad (18)$$

The Avrami theory assumed a constant nucleation rate J in order to describe simultaneous and continuous nucleation. The nucleation rate of corrosion spots of the aluminum reflector samples exposed outdoors has been determined by periodic measurements. The nucleation rate J was approximated by counting the new corrosion spots Δn that appeared during the time interval Δt in relation to the non-corroded surface area

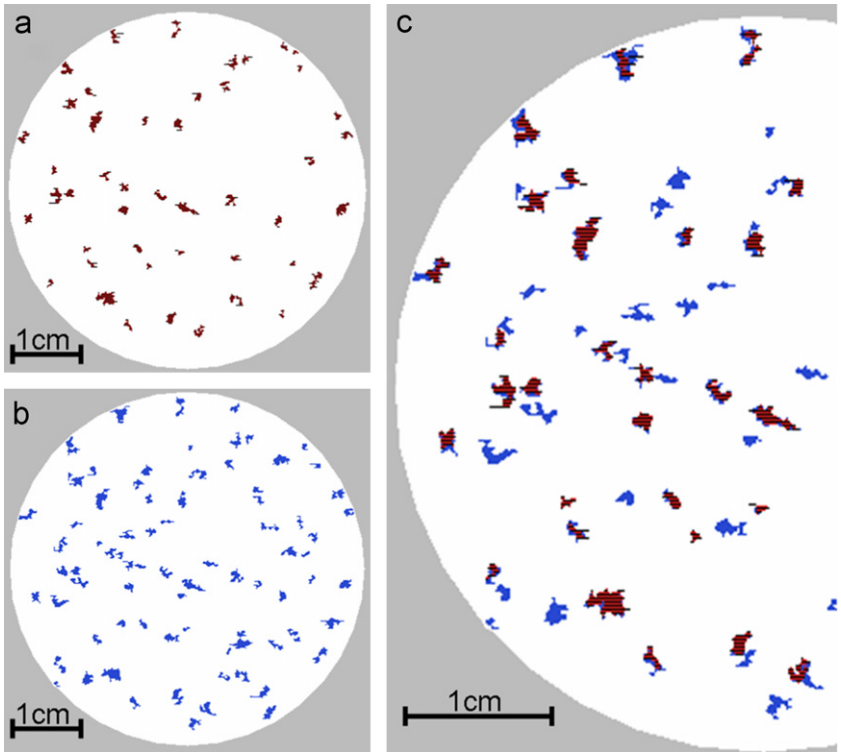

Fig. 11. Localized corrosion spots at an enhanced aluminum reflector sample without the nanocomposite layer (a) after 1 week, (b) after 2 weeks of outdoor weathering in Almería, and (c) overlayed image of (a) and (b).

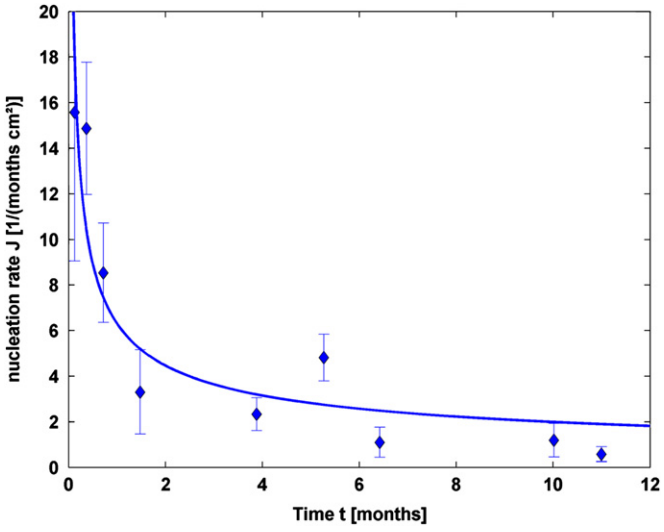

Fig. 12. Measured nucleation rate J of localized corrosion due to outdoor weathering in Almería for enhanced aluminum reflector samples without nancocomposite coating.

$(1-f_C)\,A_{total}$:

$$J=\frac{1}{A_{total}}\frac{dn_{ext}}{dt}=\frac{1}{A_{total}(1-f_C)}\frac{dn}{dt}\approx\frac{1}{A_{total}(1-f_C)}\frac{\Delta n}{\Delta t} \tag{19}$$

Fig. 12 shows the measured nucleation rate J according to Eq. (19).

The measurements show that the nucleation rate cannot be regarded as constant. The nucleation rate is modeled according to:

$$J=\frac{c_J}{\sqrt{t}}\rightarrow J\sim t^{-1/2} \tag{20}$$

where c_J is a constant. For samples without nancocomposite coating exposed in Almería c_J has been determined with least square analysis to 6.31 months$^{-0.5}$ cm^{-2}. Note that in order to derive the JMAK Eq. (12) no assumptions of the nucleation rate J were made. Thus, the JMAK equation can be applied whether J is constant or not. The corroded area fraction can then be described (from Eq. 18) as

$$f_C=1-\exp(-\pi r_{eq}^2 Jt)=1-\exp\left(-\pi r_{eq}^2\frac{c_J}{\sqrt{t}}t\right)=1-\exp(-k\sqrt{t}). \tag{21}$$

Thus an Avrami exponent of $\eta=0.5$ is obtained. According to Table 1 an Avrami exponent of $\eta=1$ or $\eta=0$ would have been expected depending on whether the nucleation is continuous or simultaneous. In reality, the nucleation appears to be in between the continuous and simultaneous case. Coating defects that occur during the manufacturing of the samples account for the simultaneous case; coating defects that are introduced during the outdoor exposure due to climatic influences account for the continuous case (see also Section 4). With the $\eta=0.5$-approach, the nucleation is modelled as a mixture of the two ideal cases.

The Avrami constant $k=\pi r^2{}_{eq}c_J$ depends on the quality of the nanocomposite coating and the climatic conditions of the outdoor exposure site. The Avrami constant can be determined by applying a least square fit to the measured data. Fig. 13 shows the measured corroded surface fraction f_C for samples without nanocomposite coating exposed in Almería. The obtained Avrami constant was $k=0.0527$ months$^{-0.5}$. The equivalent radius of the corrosion spots resulted in $r_{eq}=k^{0.5}(\pi c_J)^{-0.5}=515.6$ μm.

It is of particular interest to what extent the growing corroded surface fraction affects the specular reflectance properties of the aluminum mirror. The specular reflectance of the corroded area of samples that have been exposed at different weathering sites has

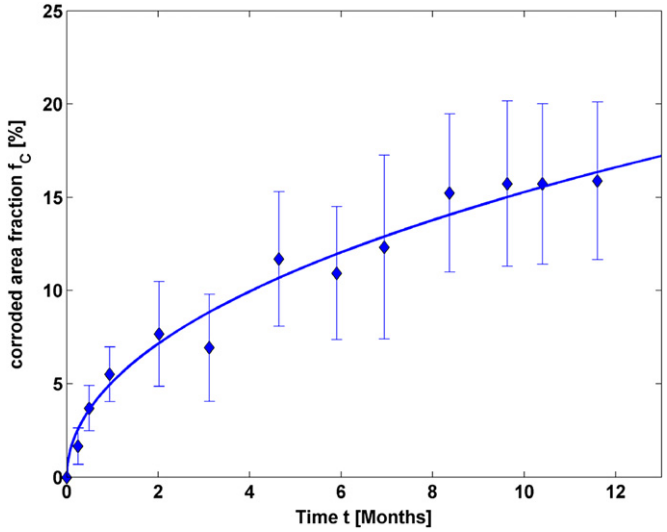

Fig. 13. Corroded area fraction f_C of enhanced aluminum reflector samples without nanocomposite coating exposed in Almería. The distribution was modelled according to Eq. (21).

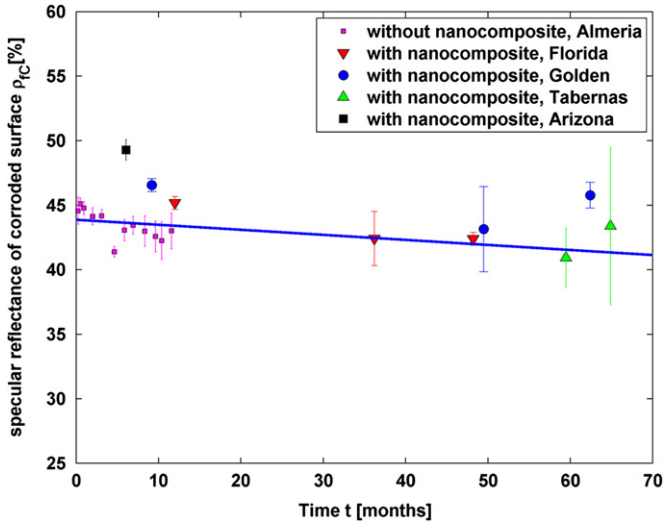

Fig. 14. Specular reflectance of the corroded surface ρf_C of different enhanced aluminum reflector samples during outdoor exposure at different sites.

been measured with the space resolved specular reflectometer (see Fig. 14).

The specular reflectance of the corroded area fraction f_C is modelled by a linear decay:

$$\rho_{fC}(t) = \rho_{0,fC} - m_C t = 44.1\% - 0.04\%\ \mathrm{t/months} \tag{22}$$

Finally, with Eqs. (21) and (22) the specular reflectance loss caused by corrosion $\Delta\rho_C$ is modelled by:

$$\Delta\rho_C(t) = f_C(t)(\rho_0 - \rho_{fC}(t)) = (1-\exp(-k\sqrt{t}))(\rho_0 - \rho_{0,f_C} + m_C t)$$
$$= (1-\exp(-k\sqrt{t}))(\rho_0 - 44.1\% + 0.04\%\ \mathrm{t/months}) \tag{23}$$

The initial specular reflectance ρ_0 of samples without nanocomposite coating is higher than for coated samples. It has been measured as:

$$\rho_0 = \begin{cases} 83.5\% & \text{for samples with nanocomposite} \\ 86.5\% & \text{for samples without nanocomposite} \end{cases} \tag{24}$$

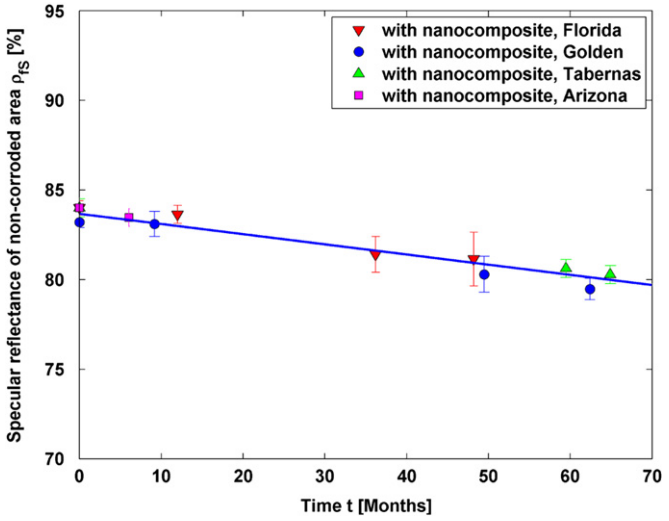

Fig. 15. Specular reflectance at $\lambda = 656$ nm, $\theta = 15^\circ$, $\varphi = 12.5$ mrad of non-corroded area for various enhanced aluminum reflector samples exposed at different sites.

Applying a least square fit to the measured corroded area fractions f_c the following Arami constants have been obtained:

$$k = \begin{cases} 5.3 \times 10^{-2}\ \mathrm{months}^{-0.5} & \text{for samples without nanocomposite in Almeria, Spain} \\ 1.1 \times 10^{-3}\ \mathrm{months}^{-0.5} & \text{for samples with nanocomposite in Tabernas, Spain} \\ 6.4 \times 10^{-3}\ \mathrm{months}^{-0.5} & \text{for samples with nanocomposite in Florida, USA} \\ 2.9 \times 10^{-3}\ \mathrm{months}^{-0.5} & \text{for samples with nanocomposite in Golden, USA} \end{cases} \tag{25}$$

3.2. Modelling of specular reflectance losses caused by scattering $\Delta\rho_S$

The non-corroded part of the surface $f_S = (1 - f_c)$ has also been analyzed with the space resolved reflectometer. Losses in specular reflectance are due to the increased surface roughness of the top coating, which introduces scattering. Fig. 15 shows the measured specular reflectance values at various exposure sites. The distribution is also modelled with a linear decay:

$$\rho_{fS} = \rho_0 - m_S t = \rho_0 - 0.057\%\ \mathrm{t/months} \tag{26}$$

The initial specular reflectance ρ_0 can be obtained from Eq. (24).

The specular reflectance loss caused by scattering $\Delta\rho_S$ is modelled by

$$\Delta\rho_S(t) = f_S(t)\ \left(\rho_0 - \rho_{fS}(t)\right) = \exp\left(-k\sqrt{t}\right) m_S t$$
$$= \exp\left(-k\sqrt{t}\right) 0.057\%\ \mathrm{t/months} \tag{27}$$

3.3. Modelling of the time dependant specular reflectance ρ

Eqs. (2), (23) and (27) result in the specular reflectance $\rho(t)$:

$$\rho(t) = \rho_0 - \Delta\rho_C(t) - \Delta\rho_S(t)$$
$$= \rho_0 - f_C(\rho_0 - \rho_{fC}) - f_S\,(\rho_0 - \rho_{fS})$$
$$= \rho_0 - f(\rho_0 - \rho_{fS}) - (1 - f_C)\,(\rho_0 - \rho_{fS})$$
$$= \rho_0 - (1-\exp(-k\sqrt{t}))(\rho_0 - \rho_{0,fC} + m_C t) - \exp(-k\sqrt{t}) m_S t$$
$$= \rho_0 - (1-\exp(-k\sqrt{t}))(\rho_0 - 44.1\% + 0.04\%\ \mathrm{t/months})$$
$$- \exp(-k\sqrt{t}) 0.057\%\ \mathrm{t/months} \tag{28}$$

The initial specular reflectance ρ_0 and the Avrami constant k can be obtained from Eqs. (24) and (25).

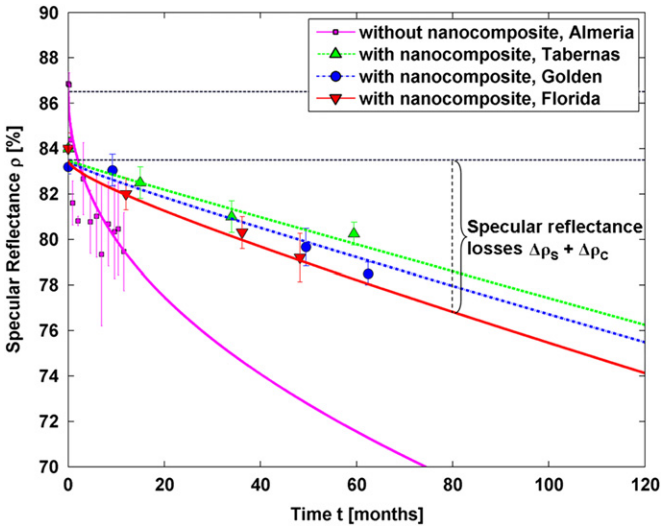

Fig. 16. Measured data of the specular reflectance ρ at $\lambda=656$ nm, $\theta=15^\circ$, $\varphi=12.5$ mrad compared to the model according to Eq. (28).

Fig. 16 shows the model according to Eq. (28) compared to measurements of different reflector samples exposed outdoors.

4. Results & discussion

For samples with protective nanocomposite top coatings Eq. (28) predicts the specular reflectance with a deviation smaller than 1 percentage point compared to the measured data after five years of outdoor exposure. Considering that the uncertainty of commercially available reflectometers lies in that rage, the model seems reasonable. However, further validation through future measurements is planned.

The fact that localized corrosion spots do not change their shape once they form is probably due to the passivation of the pure aluminum layer. The corrosion expands rapidly in a couple of hours as long as the climatic conditions permit it and if there are coating defects present. The corrosion growth might occur when the ambient humidity condensates on the reflector surface. When the electrolyte of the local cell dries out due changing climatic influences, a protective aluminum oxide layer is likely to be formed and the spot stops growing. The formation of corrosion spots is a process that occurs in day/night cycles. The changing climatic conditions also play an important role for other corrosion types. As an example, consider that filiform corrosion will only occur at a relative humidity over 65% [5].

The decay of the nucleation rate J (see Fig. 12) can be explained as follows: at the beginning of the outdoor exposure of the samples several defects in the coating, which appear during the production or transportation of the samples, initiate localized corrosion. Figs. 17 and 18 show SEM images of these types of defects for new samples with and without nanocomposite coating before outdoor weathering. Dirt particles on the surface during the coating process of the nanocomposite layer can lead to the formation of pores after the solvents evaporate. Evaporation may occur due to thermal influence or solar radiation. At this stage, nucleation is similar to the case of simultaneous nucleation described in the Avrami theory. Improved processing of recently developed nanocomposite coatings reduced manufacturing defects significantly.

During outdoor weathering new defects appear in the top coating caused by airborne dirt or dust particles or abrasive cleaning methods. These processes are similar to the case of continuous nucleation because nucleation is mainly controlled by the climatic conditions of the weathering site. This is the reason why the nucleation of corrosion spots at the enhanced aluminum reflector is described as a mixture of simultaneous and continuous nucleation ($\eta=0.5$).

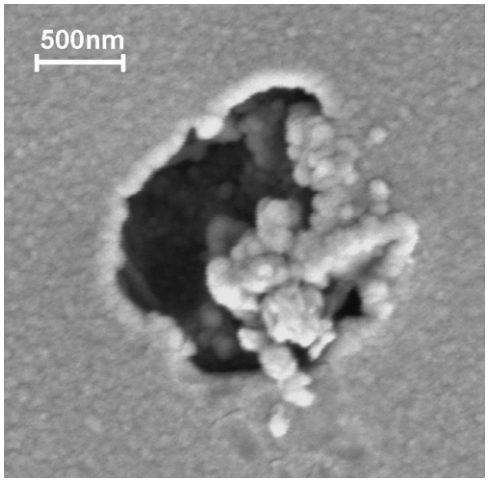

Fig. 17. Defect in new sample without nanocomposite layer.

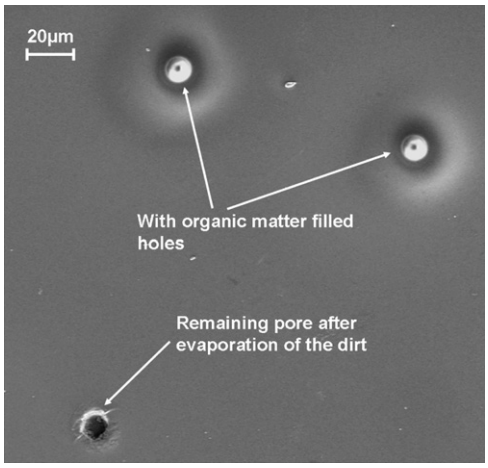

Fig. 18. Pores in a new nanocomposite coated sample.

5. Conclusions

The work presented in this article shows that the specular reflectance of enhanced aluminum reflectors is decreased by localized corrosion and scattering caused by increasing surface roughness. The corroded area can be modelled by adapting the theory of Avrami. The Avrami constant k can be obtained from outdoor exposure experiments. The constant is dependant on the exposure site. The developed model to predict the specular reflectance shows agreement with measurements from outdoor weathered samples.

After 10 years of outdoor exposure, specular reflectance losses caused by corrosion are expected to be in the range of $\Delta\rho_C=0.5$ to $3.0\pm1.4\%$ points depending on the outdoor exposure site. In the same exposure period, specular reflectance losses caused by surface roughness scattering are expected to be in the range of $\Delta\rho_S=6.6\pm1.4\%$ points. The reflectance losses caused by scattering are almost independent from the exposure site.

Future developments of transparent abrasion resistant top coatings could reduce both, corrosion initiation and specular reflectance losses caused by scattering.

Acknowledgments

The authors want to thank Cheryl Kennedy, Gary Jorgensen and Kim Jones from the National Renewable Energy Laboratory (NREL), Aranzazu Fernandez Garcia and Eduardo Zarza from the Centro de Investigaciones Energéticas, Medioambientales y Tecnológicas (CIEMAT) and Stephanie Meyen from Deutsches Zentrum für Luft- und Raumfahrt (DLR).

References

[1] T. Fend, G. Jorgensen, H. Küster, Applicability of highly reflective aluminum coil for solar concentrators, Solar Energy 68 (2000) 361–370.
[2] F. Sutter, A. Fernández, P. Heller, C. Kennedy, S. Meyen, R. Pitz-Paal, M. Schmücker, A new method to characterize degradation of first surface aluminum reflectors, in: Proceedings of the Solar PACES Conference, Perpignan. 2010.
[3] M. Avrami, Kinetics of phase change II. Transformation–time relations for random distribution of nuclei, Journal of Chemical Physics 8 (1940) 212–224.
[4] M. Fanfoni, M. Tomellini, The Johnson–Mehl–Avrami–Kolmogorov model: a brief review, Il Nuovo Cimento 20 (1998) 1171–1182.
[5] L.L. Shreir, R.A. Jarman, G.T. Burstein, Corrosion Volume 1 Metal/Environment Reactions, 3rd edition, Butterworth Heinemann, 1994, pp. 1–170 ISBN 0-7506-1077-8.